Reaction barriers on non-conducting surfaces beyond periodic local MP2: Diffusion of hydrogen on α-Al$_2$O$_3$(0001) as a test case (EP)

(iD) **Thomas Mullan**, (iD) **Lorenzo Maschio**, (iD) **Peter Saalfrank, et al.**

COLLECTIONS

Paper published as part of the special topic on Beyond GGA Total Energies for Solids and Surfaces

EP   This paper was selected as an Editor's Pick

View Online   Export Citation   CrossMark

ARTICLES YOU MAY BE INTERESTED IN

Double-hybrid density functionals for the condensed phase: Gradients, stress tensor, and auxiliary-density matrix method acceleration
The Journal of Chemical Physics **156**, 074107 (2022); https://doi.org/10.1063/5.0082327

ManyHF: A pragmatic automated method of finding lower-energy Hartree–Fock solutions for potential energy surface development
The Journal of Chemical Physics **156**, 071101 (2022); https://doi.org/10.1063/5.0080817

A consistent and accurate ab initio parametrization of density functional dispersion correction (DFT-D) for the 94 elements H-Pu
The Journal of Chemical Physics **132**, 154104 (2010); https://doi.org/10.1063/1.3382344

Reaction barriers on non-conducting surfaces beyond periodic local MP2: Diffusion of hydrogen on α-Al₂O₃(0001) as a test case

View Online   Export Citation   CrossMark

Thomas Mullan,[1] (ID) Lorenzo Maschio,[2] (ID) Peter Saalfrank,[3] (ID) and Denis Usvyat[1,a)] (ID)

AFFILIATIONS

[1] Institut für Chemie, Humboldt-Universität zu Berlin, Brook-Taylor-Str. 2, D-12489 Berlin, Germany
[2] Dipartimento di Chimica, Università di Torino, via Giuria 5, I-10125 Torino, Italy
[3] Institut für Chemie, Universität Potsdam, Karl-Liebknecht-Straße 24-25, 14476 Potsdam-Golm, Germany

Note: This paper is part of the JCP Special Topic on Beyond GGA Total Energies for Solids and Surfaces.
a) Author to whom correspondence should be addressed: denis.usvyat@hu-berlin.de

ABSTRACT

The quest for "chemical accuracy" is becoming more and more demanded in the field of structure and kinetics of molecules at solid surfaces. In this paper, as an example, we focus on the barrier for hydrogen diffusion on a α-Al₂O₃(0001) surface, aiming for a couple cluster singles, doubles, and perturbative triples [CCSD(T)]-level benchmark. We employ the density functional theory (DFT) optimized minimum and transition state structures reported by Heiden, Usvyat, and Saalfrank [J. Phys. Chem. C **123**, 6675 (2019)]. The barrier is first evaluated at the periodic Hartree–Fock and local Møller–Plesset second-order perturbation (MP2) level of theory. The possible sources of errors are then analyzed, which includes basis set incompleteness error, frozen core, density fitting, local approximation errors, as well as the MP2 method error. Using periodic and embedded fragment models, corrections to these errors are evaluated. In particular, two corrections are found to be non-negligible (both from the chemical accuracy perspective and at the scale of the barrier value of 0.72 eV): the correction to the frozen core-approximation of 0.06 eV and the CCSD(T) correction of 0.07 eV. Our correlated wave function results are compared to barriers obtained from DFT. Among the tested DFT functionals, the best performing for this barrier is B3LYP-D3.

I. INTRODUCTION

Surfaces are natural and in many cases very efficient catalysts for various types of reactions. As a result, the field of surface chemistry enjoys an intense focus from both experimental and theoretical perspectives. Due to the complexity of the processes, however, and extended nature of involved systems, the accurate theoretical description of reaction energetics is very challenging. This is especially critical for accurate calculation of reaction barriers, which, if estimated poorly, may completely undermine the subsequent kinetic modeling or reaction rate estimates. Recent attempts to achieve chemical accuracy (<1 kcal/mol) also for surface reactions are summarized in Ref. 1.

Standard computational protocols for surface reactions employ periodic super-cell models, treated with plane-wave basis sets and density functional theory (DFT), within the generalized gradient approximation (GGA). However, GGA functionals are notoriously known to substantially underestimate reaction barriers, thus in many cases providing not more than a rough estimate of the picture at hand. In a recent publication,[2] some of us demonstrated that a hybrid-DFT treatment, or Møller–Plesset second-order perturbation theory (MP2), can deliver a more realistic barrier for hydrogen diffusion on aluminum oxide surfaces. Nevertheless, the scattering of the results observed among these models was still noticeable, so a precise theoretical prediction was yet not possible. The MP2 value for the barrier, however, was between the results of different hybrid DFT functionals, allowing for a speculation that the actual barrier

is of that ballpark. However, MP2, although generally known for being accurate for oxide and ionic systems, cannot be considered a safe benchmark. In order to reach certainty about the value of the barrier (at least within reasonable margins), one has to step much higher in the hierarchy of the quantum chemical models and reach at least the coupled-cluster singles, doubles, and perturbative triples [CCSD(T)] level of theory, combined with a basis set of suitable quality.

The CCSD(T) method itself, the "gold standard" of quantum chemistry, is computationally very expensive and, when combined with good basis sets, its applicability is restricted to small molecular systems. For somewhat larger systems, usually, a hierarchical approach is employed, where the basis set limit is reached for computationally less demanding models, while the CCSD(T) correction is then computed using a more modest (although still of decent quality) basis set.[3] For even larger systems, the standard (canonical) CCSD(T) quickly becomes prohibitively expensive, even when using modest basis sets (due to the unfavorable N^7 scaling with the system size) and, thus, can only be applied with additional approximations. One of the most successful approximate CCSD(T) models applicable to extended molecules is the local CCSD(T) model.[4–12] Periodic systems add a further level of complication for high-level quantum chemical models, both of technical and fundamental nature. Until now, several effective schemes and protocols have been developed that do allow for a CCSD(T)-level treatment. First, there are some fully periodic implementations,[13,14] yet these are still very computationally demanding, especially for large unit cells, as in our case. Another possible strategy is to employ representative finite clusters, either exclusively[15,16] or for correcting a low-level periodic treatment.[17–28] However, the applicability of this approach depends on the existence of clusters that can adequately mimic the parent solid. For the system under study here—aluminum oxide—construction of such clusters is highly problematic.

In this work, we employ a different approach: the embedded fragment CCSD(T) correction, which is a powerful method for accurate description of local chemical processes in solids, for example, reactions of adsorbed species. It offers a possibility to define a fragment seamlessly via localized orbitals rather than explicit atoms, so no bond-cutting is required to create an atomic cluster. One possible realization of such an approach is to embed a wave function treatment in a DFT environment.[29–42] An alternative to the DFT embedding is the so-called Hartree–Fock (HF) embedding, where the fragment becomes implicitly embedded in the frozen Coulomb and exchange field of the true periodic HF solution. The HF description of the environment is usually not as accurate as a DFT one, especially so for metals. On the other hand, HF embedding allows us to treat the whole system in a unified seamless quantum chemical framework, operating with frozen and active orbital spaces. Conceptually, it is similar to the standard frozen-core approximation. The only difference is that here the frozen/active spaces are determined not according to the orbital energies in the canonical representation but rather on the basis of spatial proximity to the feature of interest in the direct space representation.

In recent years, periodic HF embedding has drawn substantial interest and several groups have developed various flavors of this approach.[43–48] In this work, we employ our recent interface to the Molpro code,[49,50] which passes the one-electron Hamiltonian matrix

and two-electron integrals in the basis of the fragment orbitals to the molecular code.

We use the embedded fragment to evaluate the CCSD(T) correction to the periodic local MP2 (LMP2) treatment, i.e., to correct the MP2 method error. All other significant errors of the periodic LMP2 treatment are analyzed and corrected in the periodic regime. The goal of this paper is to provide a CCSD(T) benchmark for the hydrogen diffusion barrier on α-Al$_2$O$_3$(0001) and formulate a protocol for high precision calculations of quantities relevant to the description of the kinetics of catalytic reactions on non-conducting surfaces.

II. STRUCTURES

The initial and final states of the considered reaction represent two stable geometries of dissociative water adsorption on α-Al$_2$O$_3$(0001) surface, which according to the nomenclature of Refs. 2 and 51 are marked as "1-4" and "1-2," respectively (see Fig. 1). The 1-2 structure is a global minimum for water adsorption on this surface with 1-4, according to LMP2 or B3LYP-D3, being about 0.4 eV higher in energy.[2] The reaction from 1-4 to 1-2 represents the diffusion of the hydrogen atom from one surface oxygen atom to another.

The barrier for this reaction was calculated in Ref. 2 using DFT and LMP2 methods. Even when discarding the Hartree–Fock (HF) outlier, the resulting free energy values (at 300 K) for the barrier scatter considerably: from 0.27 eV (PW91) to 0.58 eV (B3LYP-D3). The MP2 barrier was found between these values, closer to the B3LYP result. The main difference in the results was originating from the electronic contribution to the barrier, as the zero point energy (ZPE) and thermal contributions, computed with B3LYP and Perdew–Burke–Ernzerhof (PBE), are comparable (−0.11 eV vs −0.15 eV, respectively). Consequently, in this work, we focus solely on the electronic contribution to the barrier,

$$\Delta E = \Delta E^{\ddagger} = E(\text{TS}) - E(1-4). \quad (1)$$

The α-Al$_2$O$_3$(0001) surface in our calculations is represented by a nine-layer slab. Since we employ atomic-orbital (AO) basis sets, we do not replicate the slab in the $\vec{z}$-direction, commonly done in
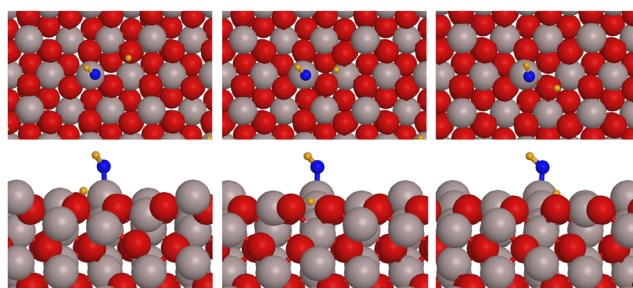

FIG. 1. Top (top) and side view (bottom) of the 1-4 geometry (left), the transition state (middle), and the 1-2 geometry (right). The adsorbed oxygen has been colored blue and reduced in radius for distinction from the surface ones.

plane-wave calculations. The 1-4 and transition state (TS) structures of Eq. (1) were taken from Ref. 2, where they were optimized with B3LYP within a 63-atom super-cell. The explicit structure specifications can be found in the supplementary material.

We note that in this work, we do not aim at investigating the possible errors due to the slab model of the aluminum oxide surface or inaccuracy of DFT structure optimizations. First, it is very difficult to go beyond a slab-model and DFT for geometry optimization, ZPEs, and thermal effects. At the same time, DFT geometries and vibrational frequencies are usually not inaccurate. Hence, the main focus is commonly put on the electronic part of the barrier energy evaluated from two single point calculations on DFT optimized structures. If it is captured with high accuracy, the overall free energy of the barrier becomes a good reference for experiment.

Second, a high precision electronic energy difference alone is a valuable benchmark for DFT. As DFT remains the only practical option for large scale calculations, benchmarking the performance of the employed functional or functionals on key quantities becomes absolutely instrumental.

III. QUANTUM CHEMICAL MODELS

In this section, we will describe in detail approximations and possible sources of error, namely, basis set choice, thresholds and truncations inherent to the approximations employed, level of theory, and fragment choice.

A. Hartree–Fock and basis sets

In this work, we calculate the barrier [Eq. (1)] using a hierarchy of quantum chemical models. We start from the periodic AO-based HF method of the Crystal code.[52] Unfortunately, rich standard molecular basis sets are usually inapplicable for periodic calculations without additional adjustment, as even slightly diffuse orbitals cause quasi-linear dependencies among basis functions and numerical instabilities in the SCF procedure. In this work, for most of the calculations, we use a VTZ-quality basis set, optimized for periodic systems, which was already employed in Ref. 2 (basis set AO3). We refer to this basis set as VTZ. The explicit specification of this basis set as well as all other basis sets used here is given in the supplementary material.

Yet, it may become possible to employ rich molecular basis sets (at least some of them) in periodic calculations, if the corresponding orbitals are placed not everywhere but only on a few selected atoms. This opens the possibility to pick up an atomic fragment spatially close to the reaction site and use a molecular basis set hierarchy for the atoms of this fragment only. In this way, we employ the cc-pVTZ and cc-pVQZ basis sets of the Dunning basis set family[53] on fragments defined below. The fragments only involve oxygen and hydrogen atoms, as cc-pVXZ basis sets for aluminum are very diffuse and not applicable, even when put on just a few atoms. Due to technical reasons (the AOs of higher angular momentum than f are not yet implemented in Cryscor), the g-AOs were omitted from the cc-pVQZ basis of oxygen. All atoms outside the chosen fragment still feature the VTZ basis.

Next, for the accurate post-HF description of dispersion, diffuse high-angular momentum orbitals are needed in the basis.[54]

We include them via the dual basis set technique,[55] i.e., only for the post-HF treatment. We denote such basis sets as (A)VTZ or (aug-)cc-pVXZ:[56] the latter correspond to the cases when the Dunning basis sets are used on the fragment atoms.

Within the dual basis set scheme, it is also possible to perturbatively estimate the contribution of the appended orbitals to the HF energy through the so-called first-order singles,[55,57]

$$\delta^{\mathrm{sing}} E_{\mathrm{HF}} = \frac{2}{N_{\mathbf{k}}} \sum_{\mathbf{k}} \frac{|f_{ai}(\mathbf{k})|^2}{\epsilon_a(\mathbf{k}) - \epsilon_i(\mathbf{k})}. \quad (2)$$

Here, $N_{\mathbf{k}}$ is the number of $\mathbf{k}$-points in the Brillouin zone sampling, $\epsilon_a(\mathbf{k})$ and $\epsilon_i(\mathbf{k})$ are the virtual and occupied orbital energies, respectively, and $f_{ai}(\mathbf{k})$ are the occupied–virtual elements of the Fock matrix, which are not all zero in the dual basis set scheme. This approach is also employed to add the tight orbitals from the cc-pwCVTZ basis set[58] for Al atoms for evaluating the correlated core contribution to the barrier (see Sec. III B 1).

B. Local MP2

For the periodic post-HF treatment, we use a local MP2 model. The closed-shell local MP2 energy may be written as

$$E_{\mathrm{corr}}^{\mathrm{LMP2}} = \sum_{ij \in \mathbb{P}} \sum_{ab \in [ij]} \left(2T_{ab}^{ij} - T_{ba}^{ij} \right)(ia|jb). \quad (3)$$

Here, i and j are the localized occupied orbitals, a and b are the localized virtual orbitals, and $(ia|jb)$ are two-electron integrals in the chemical notation,

$$(ia|jb) = \iint d\mathbf{r}_1 d\mathbf{r}_2 \varphi_i(\mathbf{r}_1)\varphi_a(\mathbf{r}_1)\frac{1}{r_{12}}\varphi_j(\mathbf{r}_2)\varphi_b(\mathbf{r}_2), \quad (4)$$

and T_{ab}^{ij} are the MP2 amplitudes obtained by solving the MP2 equations.[59,60] First, we note that in the local (direct space) representation, the orbitals are real, so there is no need to explicitly specify the complex conjugation in (4). Second, in contrast to the canonical basis, the local MP2 equations are not trivially invertible. However, these equations are linear and an iterative LMP2 equation solver usually converges quickly.

In (3), the summation ranges are denoted as $\mathbb{P}$, which represents the pair-list for the occupied orbitals, and $[ij]$ for the virtual orbitals specific for each occupied orbital pair ij. In the direct space representation for the correlation energy per cell, one of the indices (e.g., "i") has to be restricted to the reference cell. An additional restriction of other indices implies an approximation to the MP2 method. In this work, we will explore the effect of the involved approximations that truncate the pair list and virtual space.

1. Frozen core

We start with the frozen core approximation, very common in correlated calculations, which restricts the pair-list $\mathbb{P}$ to the valence occupied orbitals only. It assumes cancellation of the core–valence and core–core correlation contribution in energy differences related

to chemical processes. Although this assumption is generally reasonable, the influence of the core correlation associated with the high core orbitals of the metal atoms (in our case 2s2p-core of Al) may not be entirely negligible. We investigate this by comparing the periodic LMP2 barriers with and without the 2s2p-core of Al atoms correlated,

$$\delta^{core}\Delta E_{corr}^{LMP2} = \Delta E_{corr}^{LMP2}(FC_{1s}) - \Delta E_{corr}^{LMP2}(FC), \tag{5}$$

where "FC" stands for the "frozen core," and "FC_{1s}" denotes that only 1s-core of oxygen and aluminum atoms is kept frozen. These calculations employ the (C)VTZ and (AC)VTZ basis sets that contain the special tight orbitals from the cc-pwCVTZ basis of the Al atoms.[58]

2. Pair approximation

Next, we focus on the so-called local approximations. The first approximation of this kind is the pair-approximation that further restricts the pair-list. In molecular local correlation methods, the pair-list is truncated for efficiency reasons (in particular, to reach linear scaling), as the pair-energy contributions decay with the inverse sixth power of the distance between the centers of the local orbitals.[9,61] In a periodic system, it is in principle not possible to include all Wannier function (WF) pairs in the pair-list $\mathbb{P}$, even formally, as their number is infinite. In order to investigate the influence of the pair approximation, we progressively expand the pair-list until convergence of ΔE_{corr}^{LMP2} is achieved.

3. Domain approximation

The second essential local approximation is the so-called domain approximation, which restricts the virtual space for each pair ij to the pair domains $[ij]$. A pair domain is thus a pair-specific set of virtual orbitals.

In this work, we use two types of virtual orbitals and, therefore, two types of pair domains. The virtuals of the first type are the projected atomic orbitals (PAOs).[57,62] These orbitals are AOs, which are projected out from the occupied manifold and so are atom-centered. A PAO pair domain $[ij]$ consists of all PAOs, centered on the atoms, that are spatially close to the occupied orbitals i or j of a pair. It is convenient to define the minimal PAO domains, which include PAOs from only one atom (for lone-pair WFs) or two atoms (for bond WFs) per occupied orbital. The domains can then be systematically expanded by adding the PAOs from nearest-neighbor atoms (iext = 1), second-nearest-neighbor atoms (iext = 2), etc. In aluminum oxide, which is to a large extent ionic, the WFs are centered on oxygens, so the corresponding minimal domains consist of the PAOs of just single oxygen atoms. Extension to the nearest-neighbors (iext = 1) adds a shell of the aluminum atoms surrounding the initial oxygen, and a second nearest-neighbor (iext = 2) is the next shell of the oxygen atoms.

Restriction of the virtual space to the PAO pair-domains leads to a compact pair-specific virtual space, and, at the same time, a common global set of virtual orbitals remains, which facilitates calculation of integrals and other intermediates. Yet, a known issue of PAO-based domains is a possible imbalance between the virtual

spaces for different points on the potential energy surface, at least when small domains are used. The reason is that the virtual space can be varied only rather coarsely, by adding or removing *all* the PAOs of a given atom.

As an alternative to PAOs, in periodic local MP2, one can also use the so-called orbital specific virtuals (OSVs).[63,64] OSVs for a given occupied orbital i are defined as the MP2 virtual natural orbitals for a diagonal pair ii. To truncate the virtual space by including only the essential OSVs, an energy cutoff is usually used (in Cryscor 10^{-5} hartree by default). An OSV pair-domain for a non-diagonal pair ij is defined as a union of the OSVs corresponding to the orbitals i and j. There is also one aspect that is specific to our OSV implementation: in order to counterbalance the bias of the OSVs toward the short-range correlations, the most diffuse PAOs of the corresponding minimal PAO domain (one shell of PAOs per angular momentum per center) are added to the set of the OSVs.

The OSVs and, thus, the OSV domains automatically adapt to the change in the structure, so the imbalance and discontinuity of the potential surface are much weaker than with PAO domains. On the downside however, with OSVs, it turns out to be difficult to explore convergence with domain size in periodic calculations, as tightening of the cutoff energy threshold requires progressive expansion of the fitting basis.[64]

4. Density fitting

The next approximation in the periodic local MP2 method concerns the evaluation of the electron repulsion integrals $(ia|jb)$ of Eq. (4). These integrals are used both in the LMP2 energy expression [Eq. (3)] and in the LMP2 amplitude equations.[60] In order to gain efficiency, they are not evaluated and transformed as 4-index AO integrals but rather assembled from 3- and 2-index quantities by means of the density fitting (DF) approximation. In our approach, we use local robust density fitting, which is very efficient in bulk systems.[65,66] Yet, this is an approximation, as the integrals are not exact. DF is known to be generally very accurate for energy differences. It is, however, of interest to check its accuracy also for this system.

The DF approximation in MP2 implies decomposition of occupied–virtual orbital products $\rho_{ia}(\mathbf{r}) = \varphi_i(\mathbf{r})\varphi_a(\mathbf{r})$ in an auxiliary (or fitting) basis $\{\phi_P\}$,[65,66]

$$\rho_{ia}(\mathbf{r}) = \sum_{P \in [ia]_{fit}} d_{ia}^P \phi_P, \tag{6}$$

where $[ia]_{fit}$ is the fitting domain that includes the fitting functions centered on the atoms supporting the product density $\rho_{ia}(\mathbf{r})$. As the fitting functions, we use Poisson-type orbitals (PTOs),[65,67,68] directly converted from the MP2-optimized Gaussian-type-orbital (GTO) fitting basis sets.[65] In addition to the momentless PTOs, in order to capture the moments of the fitted product densities, the PTO fitting basis sets are appended with a few GTOs: one shell per angular momentum per center in the fitting-domain (s-type GTOs are not included, as the densities ρ_{ia} are chargeless).

In the calculations presented here, we used the PTO basis converted from the GTO fitting basis set optimized for MP2 with aug-cc-pVTZ orbital basis.[69] In order to check the accuracy of the

DF approximation, we compared these results against those calculated with aug-cc-pV5Z-optimized fitting basis sets. The deviation in ΔE_{corr}^{MP2} between these two fitting basis sets was less than 10^{-5} eV, suggesting that the error due to the density fitting approximation is absolutely minute.

5. Local correlation partitioning

The local correlation scheme allows not only for a highly efficient correlated treatment, but it also enables partitioning of correlation part of the interaction energies into physically interpretable components. Usually, such partitioning is used in the context of inter-molecular interactions, where one can isolate the inter-molecular as well as intra-molecular components of the interaction energies. In our approach, we also employ a similar partitioning scheme to investigate how much of the correlated correction to the barrier stems from the correlation inside the fragments (see Secs. III D and III C).

According to Eq. (3), the total correlation energy can be defined via the pair energies,

$$e_{ij} = \sum_{ab\in[ij]} \left(2T_{ab}^{ij} - T_{ba}^{ij}\right)(ia|jb). \tag{7}$$

With this, the correlation energy and, thus, the correlation part of the barrier can be partitioned into the intra-fragment, extra-fragment, and inter-fragment-environment components,

$$E_{corr}^{LMP2} = E_{intra-frag} + E_{extra-frag} + E_{inter}, \tag{8}$$

with

$$E_{intra-frag} = \sum_{i\in frag, j\in frag} e_{ij}, \tag{9}$$

$$E_{extra-frag} = \sum_{i\notin frag, j\notin frag} e_{ij}, \tag{10}$$

$$E_{inter} = \sum_{i\in frag, j\notin frag} e_{ij} + \sum_{i\notin frag, j\in frag} e_{ij}. \tag{11}$$

Furthermore, different pair restriction thresholds can be applied to different pair classes individually. In this way, the pair classes that do not contribute substantially to the quantity of interest (in our case the barrier) can be restricted more harshly. This allows for substantial gains in efficiency without affecting the accuracy.

6. Basis set convergence of the correlation energy

It is well known that the correlation energy is sensitive to the basis set quality. Therefore, it is essential to estimate the basis set limit for the correlated part of the barrier, instead of just remaining at the AVTZ basis set level (as in Ref. 2). To this end, we employ two techniques. First, we extrapolate ΔE_{corr}^{LMP2} using the standard inverse-cubic formula.[70] The extrapolation is based on the results with the (aug-)cc-pVTZ and (aug-)cc-pVQZ basis sets placed on the fragment atoms (see Subsection III D). The basis set extrapolation is done with both the PAO and OSV approaches. The second scheme

for ΔE_{corr}^{LMP2} at the basis set limit is the periodic LMP2-F12 method, which, at this point, is only implemented with PAOs.[66]

C. CCSD(T) correction

Finally, in order to approach chemical accuracy, we also need to correct for the MP2 method error itself. Here, the correlated treatment is extended to the CCSD(T) level via the embedded fragment approach. In this method, a group of localized occupied and virtual orbitals from the periodic calculation, which are spatially close to the reaction, define a fragment. The embedding of the fragment in the periodic HF solution is incorporated in the fragment's one-electron Hamiltonian h_{pq}^{frag}, which is constructed from the periodic Fock matrix F^{cryst} and includes the Coulomb and exchange potential from the rest of the crystal,[50]

$$h_{pq}^{frag} := F_{pq}^{cryst} - \sum_{i\in frag}^{occ} [2(pq|ii) - (pi|iq)], \tag{12}$$

$$= h_{pq}^{cryst} + \sum_{i\notin frag}^{occ} [2(pq|ii) - (pi|iq)], \tag{13}$$

where p and q (as well as r and s below) are the general orbitals of the fragment (occupied or virtual). The two-electron part of the fragment Hamiltonian elements $(pq|rs)$ is computed in Cryscor using the localized orbitals from the actual periodic calculation.[50] Importantly, the fragment orbitals are, by construction, orthogonal to the occupied orbitals of the environment, allowing for a clean and seamless cut between the fragment and embedding spaces.

The Hamiltonian matrix elements h_{pq}^{frag} and $(pq|rs)$ are transferred to the molecular code Molpro[71] via a FCIDUMP interface,[72] where any available canonical post-Hartree–Fock treatment can be applied. The method correction is then defined as

$$\delta^{meth}\Delta E = \Delta E_{emb.frag.}^{meth} - \Delta E_{emb.frag.}^{MP2}. \tag{14}$$

As noted above, the focal high-level method for the correction, denoted by "meth" in (14), is CCSD(T), providing $\delta^{CCSD(T)}\Delta E$. We will, however, also test other less expensive methods, such as CCSD and distinguishable cluster with singles and doubles (DCSD).[73–75]

D. Specification of the fragments

As discussed above in Secs. III A and III C, we employ fragments for the basis set extrapolation of the correlation energy and for the evaluation of $\delta^{CCSD(T)}\Delta E$. We use three fragments of progressively increasing size, which is shown in Fig. 2. The oxygen atoms of the fragments are marked in blue.

For the basis set extrapolation, the atomic orbitals of the (aug-)cc-pVTZ or (aug-)cc-pVQZ basis set are placed on the fragment oxygen and hydrogen atoms. The rest, including all aluminum atoms, remain with the (A)VTZ basis. The standard Dunning basis sets of aluminum contain too diffuse AOs that cannot be used for periodic calculations. However, since all the valence WFs are localized on oxygen atoms, a triple-zeta basis set level for aluminum is expected to be sufficient.
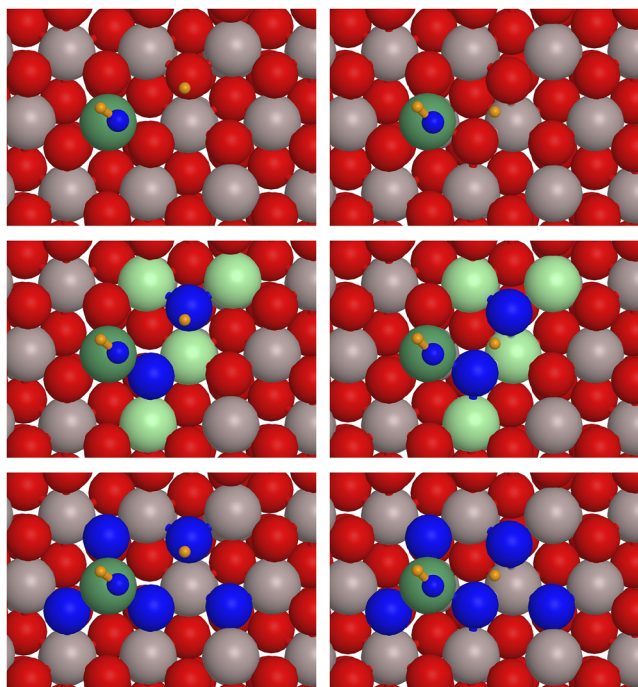
FIG. 2. Fragments 1 (top), 2 (middle), and 3 (bottom) geometries. The left picture refers to the 1-4 geometry and the right to the TS geometry. The oxygen atoms belonging to the fragments are colored blue. The atoms marked green are the aluminum atoms of the fragments used for the MP2 method error correction. By light green, we marked the aluminum atoms of Fragment 2 with the extended virtual space. Since the valence WFs are centered exclusively on oxygens, the aluminum atoms add only virtual functions to the fragment spaces via the respective PAOs.

For the embedded fragment treatment, the fragments are defined by the valence WFs, which are centered on the marked oxygen atoms: four per atom. The fragment's virtual space is spanned by the PAOs from the minimal domains of these WFs (see Sec. III B 3). This includes the PAOs of the oxygen atoms of the fragment, the hydrogen atoms, and one aluminum atom bound to the adsorbed OH group. For the VTZ basis and Fragment 2, we also expanded the virtual basis to the PAOs from the next nearest-neighbor atoms, which added another four aluminum atoms (see Fig. 2). Table I summarizes the specification of the occupied and virtual space in the fragments.

We note that the actual number of the orthogonal virtual orbitals of the fragment is slightly smaller than the number of PAOs. In fact, PAOs form a non-orthogonal and even generally redundant set (as by construction there are as many PAOs as AOs). Before the in-fragment canonicalization, the fragment's PAOs are orthogonalized, employing the same procedure as in PAO-based local correlation methods.[76] It takes the eigenvectors of the PAO overlap matrix as the orthonormal virtual set to be canonicalized. However, to get rid of linear dependencies (or quasi-linear dependencies), all the eigenvectors with the eigenvalues below a certain threshold (the default value in Cryscor is 10^{-4}) are excluded.

TABLE I. Summary of the occupied and virtual spaces for the different fragments under consideration.

Fragment	1	2	2 (ext. virt. space)	3
No. of occ. orbitals	4	12	12	24
No. of PAO atoms	4	6	10	9
VTZ				
No. of PAOs	97	157	313	247
No. of orthog. virtuals	94	151	301	236
(A)VTZ				
No. of PAOs	121	205		331
No. of orthog. virtuals	118	199		320

IV. RESULTS AND DISCUSSION

We start our discussion with the HF barriers. Table II summarizes the values for ΔE_{HF} obtained with different basis sets. The diffuse orbitals were added only within the dual basis set approach; hence, their contribution was captured via the singles correction of Eq. (2).

As follows from Table II, the HF barrier is not very sensitive to the basis set level, at least starting from (A)VTZ. However, there is scattering of the results of about 0.02 eV, with no clear convergence pattern. For estimating ΔE_{HF}, we take the value of 1.13 eV, which was obtained using the (aug-)cc-pVQZ basis on the biggest fragment [and (A)VTZ on the rest]. However, due to the singles scatter, the uncertainty cannot be reduced to less than 0.02 eV. As noted above and will also be seen later, the HF barrier is much too high when compared to the correlated methods.

Next, we move on to the correlation energy contribution to the barrier, where we first focus on the periodic local MP2 treatment. In Fig. 3, we analyze the locality of the correlation effect on the barrier using LMP2(OSV)/(A)VTZ. For Fragment 1, the intra-fragment contribution is virtually zero, suggesting that the electron correlation of the electrons near the OH group does not influence the barrier. However, already for Fragment 2, $\Delta E_{\text{intra-frag}}$ becomes the dominant component of $\Delta E_{\text{corr}}^{MP2}$. This suggests that with fragments 2 and 3,

TABLE II. The periodic HF contribution to the barrier ΔE_{HF} in eV computed using different basis sets and fragments (see Secs. III A and III D for detailed specifications).

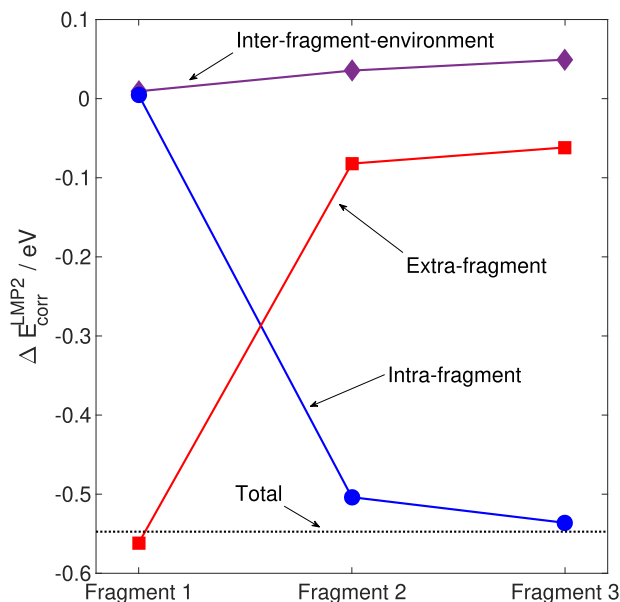|	HF	Singles	HF + singles
(A)VTZ	1.166	−0.029	1.137
(aug-)cc-pVTZ			
Fragment 1	1.165	−0.025	1.140
Fragment 2	1.170	−0.037	1.133
Fragment 3	1.166	−0.029	1.137
(aug-)cc-pVQZ			
Fragment 1	1.166	−0.018	1.149
Fragment 2	1.161	−0.011	1.150
Fragment 3	1.156	−0.028	1.129

FIG. 3. The LMP2(OSV)/(A)VTZ correlation energy components $\Delta E_{\text{intra-frag}}$, $\Delta E_{\text{extra-frag}}$ and ΔE_{inter}, calculated with the three different fragment definitions (see Sec. III D for the exact specification). For each fragment, the energy components sum up to the same total energy [$\Delta E_{\text{corr}}^{\text{LMP2}}$(OSV) = −0.547 eV], as the same cutoff radii $R_{\max}^{\text{intra-frag}} = R_{\max}^{\text{extra-frag}} = R_{\max}^{\text{intra}} = 12$ Å were taken.

TABLE IV. The basis set extrapolated $\Delta E_{\text{corr}}^{\text{LMP2}}$ values computed with PAOs (iext = 2 domains) and OSVs. The basis set extrapolation was performed using the correlation energies obtained with the (aug-)cc-pVTZ and (aug-)cc-pVQZ basis functions placed on the fragment atoms [the rest remaining (A)VTZ]. For the fragment specification, see Sec. III D.

	Fragment 1	Fragment 2	Fragment 3
$\Delta E_{\text{corr}}^{\text{LMP2}}$(PAO) (eV)	−0.549	−0.536	−0.536
$\Delta E_{\text{corr}}^{\text{LMP2}}$(OSV) (eV)	−0.555	−0.544	−0.542

Conversely, the resulting energies depend much stronger on the PAO-domains. In Fig. 4, we show the basis set limit estimates for $\Delta E_{\text{corr}}^{\text{LMP2}}$ obtained with the basis set extrapolation and LMP2-F12 method using different PAO domains. For the minimal domains (iext = 0) and especially for the iext = 1 domains, the results depend strongly on the scheme employed to approach the limit. For iext = 2 domains, on the other hand, the extrapolated and F12 results agree as they agree also with the OSV-based calculations.

The problem occurring with smaller domain calculations seems to be related not to the dependence of the barrier on the basis set but rather to the imbalance between the virtual space of the 1-4 and transition state structures. This follows from the fact that the correction on top of the (A)VTZ value turns out to be rather small: +0.003 eV for the extrapolation and 0.016 eV for F12 (see the supplementary material). The OSV approach is much less prone to the imbalance issues, as the virtual orbitals naturally adapt to the change in the structure. We, therefore, take the OSV
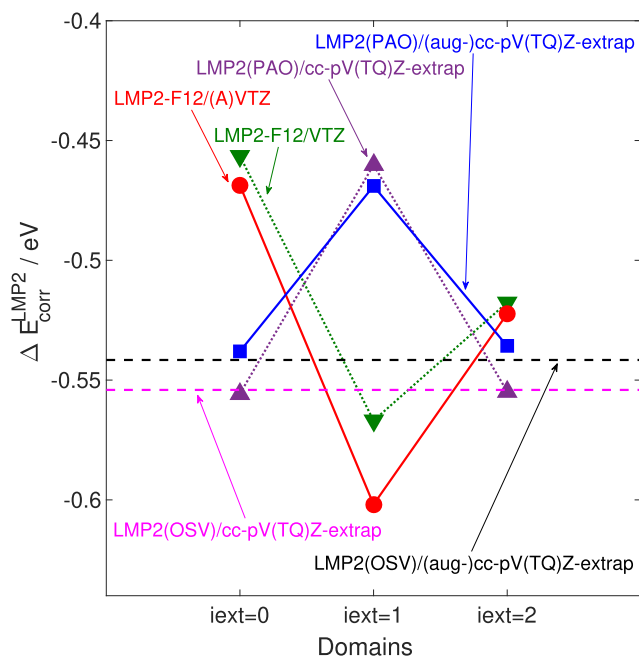
an accurate description of the intra-fragment correlation would also provide an accurate overall description.

As a next step, we explore the accuracy and possible sources of errors in the periodic LMP2 treatment due to the additional approximations. First, as may be seen from Table III, $\Delta E_{\text{corr}}^{\text{MP2}}$ converges relatively fast with the pair-list cutoff distance, suggesting that the pair approximation does not introduce any sizable error.

The domain error, however, is more difficult to estimate and eliminate, predominantly so in the PAO approach. Since the domain error and the basis set incompleteness error are of the same origin (due to restriction of the virtual space), we treat these two errors together. First, we note that, according to Table IV, the basis set extrapolated value depends very mildly on the fragment that features the actual (aug-)cc-pVTZ and (aug-)cc-pVQZ basis functions.

TABLE III. Dependence of the LMP2(OSV)/(A)VTZ correlation contribution to the barrier on the pair-list truncation. The cutoff distances for different pair classes are given in Å. The partitioning into intra-fragment, extra-fragment, and inter-pairs was done on the basis of Fragment 3.

$R_{\max}^{\text{intra-frag}}$	$R_{\max}^{\text{extra-frag}}$	$R_{\max}^{\text{inter}}$	$\Delta E_{\text{corr}}^{\text{LMP2}}$ (eV)
6	2	2	−0.727
8	4	4	−0.541
10	6	6	−0.546
12	8	12	−0.547

FIG. 4. The basis set limit estimates for $\Delta E_{\text{corr}}^{\text{LMP2}}$ calculated using the basis set extrapolation (with the Dunning basis sets placed on the atoms of Fragment 3) and the periodic LMP2-F12 method. The PAO results were obtained with the minimal (iext = 0) and extended (iext = 1 and iext = 2) domains.

(aug-)cc-pV(TQ)Z-extrapolated value of −0.54 eV as the MP2 reference result. This value also does not deviate strongly from the iext = 2 PAO results: 0.006 eV from the PAO extrapolated result and 0.019 eV from the LMP2-F12 value. However, the 0.02 eV discrepancy has to be taken into account as a possible uncertainty of the result.

Next, we draw our attention to the core correlation. The frozen core approximation is standard in most post-HF applications, but when aiming at very high precision, the core correlation contribution may be non-negligible.[28,77–79] This is apparently also the case here: when the 2s2p electrons of aluminum are correlated, $\delta^{core}\Delta E_{corr}^{LMP2}$ adds around +0.06 eV, regardless whether PAOs, OSVs, or (AC)VTZ or (C)VTZ are used (see Table 7 of the supplementary material for the detailed results).

Finally, we correct the MP2 method error by evaluating the $\delta^{CCSD(T)}$ correction. Table V compiles the values for the correction computed for different fragments and basis sets. The CCSD(T)-correction to MP2 of +0.07 eV is not negligible and (if excluding Fragment 1, which is clearly too small and inadequate for this system) remains very stable across the fragments and basis sets.

We also tested a few other methods for the method correction: CCSD, DCSD, and the spin-component-scaled-(SCS-)DCSD.[75] CCSD noticeably overestimates barrier, as $\delta^{CCSD}\Delta E$ is approximately twice as large as $\delta^{CCSD(T)}\Delta E$. DCSD results are much closer to CCSD(T), especially so with the SCS version of DCSD, which virtually coincides with CCSD(T). Interestingly, the dependence of the correction on the fragment is stronger for CCSD or DCSD than for CCSD(T) but is still rather weak.

Having thus examined and eliminated the main errors in the quantum chemical treatment, we are in a position to provide the benchmark value for the barrier for hydrogen diffusion from the 1-4 to 1-2 structures on the aluminum oxide surface, which amounts to 0.72 eV. In Table VI, we compile the final results and compare them to the DFT values of Ref. 2. It is clear that the HF barrier is much too high. The MP2 result is of reasonable quality, but when using the frozen core approximation, the barrier is yet substantially lower than the reference. The core correlation and CCSD(T) corrections

TABLE V. The $\delta^{meth}\Delta E$ correction (see Sec. III C) computed using the embedded fragment approach with different high-level methods, fragments (see Sec. III D for specification), and VTZ and (A)VTZ basis sets. All energies are in eV.

Fragment	1	2	2 Ext. virt. space	3
$\delta^{CCSD}\Delta E$(VTZ)	−0.002	0.140	0.141	0.150
$\delta^{CCSD}\Delta E$((A)VTZ)	−0.002	0.143		0.155
$\delta^{DCSD}\Delta E$(VTZ)	−0.001	0.100	0.101	0.107
$\delta^{DCSD}\Delta E$((A)VTZ)	−0.001	0.102		0.113
$\delta^{SCS-DCSD}\Delta E$(VTZ)	−0.000	0.064	0.065	0.067
$\delta^{SCS-DCSD}\Delta E$((A)VTZ)	−0.000	0.066		0.073
$\delta^{CCSD(T)}\Delta E$(VTZ)	−0.001	0.072	0.071	0.073
$\delta^{CCSD(T)}\Delta E$((A)VTZ)	−0.001	0.072		0.073

TABLE VI. The electronic barrier for the hydrogen diffusion 1-4 → 1-2 ΔE calculated at the different levels of theory. The "HF" value corresponds to the periodic HF+singles results using the (aug-)cc-pVQZ on Fragment 3 and (A)VTZ on the rest. By "MP2(FC)," we denote the OSV-based frozen-core periodic LMP2 result extrapolated using (aug-)cc-pV(TQ)Z on Fragment 3. The "MP2" result is "MP2(FC)" plus the 2s2p-Al-core correlation correction $\delta^{core}\Delta E^{MP2}$. "CCSD," "DCSD," "SCS-DCSD," and "CCSD(T)" denote the "MP2" result plus the embedded fragment correction $\delta^{meth}\Delta E$ at the respective level. The DFT values are taken from Ref. 2. The B3LYP value is obtained directly from B3LYP-D3 by subtracting the D3 contribution.

Method	ΔE (eV)
HF	1.13
MP2(FC)	0.59
MP2	0.65
CCSD	0.81
DCSD	0.76
SCS-DCSD	0.72
CCSD(T)	0.72
B3LYP-D3	0.69
B3LYP	0.65
HSE06	0.56
PW91	0.42
PBE-D2	0.44

are both noticeable and of the same sign, accumulating the error of MP2 with the frozen core.

Among the DFT functionals, the hybrids are clearly better performing than GGAs, which grossly underestimate the barrier. Interestingly, the B3LYP-D3 value is very close to our benchmark. The dispersion contribution to the barrier is not negligible but fairly small, as is revealed by the D3 component amounting to +0.04 eV. The quick convergence of the LMP2 barrier and the post-MP2 corrections with the fragment size suggests that the essential dispersion part comes from the region directly surrounding the reaction. For such a reaction, where the reactant and the product are both adsorbed on a surface, the long range dispersion contributions are indeed expected to cancel out to a large extent in the energy differences.

V. CONCLUSIONS

The goal of this contribution is two-fold. First, we report a highly accurate benchmark value of 0.72 eV for the barrier of hydrogen diffusion on α-Al_2O_3(0001) surface. The main uncertainty originates in the basis set convergence, which could not be reduced below 0.02 eV, both in HF and in MP2. However, even if these errors accumulate, it still remains within chemical accuracy. The GGA DFT barriers in comparison to this benchmark are clearly severely underestimated: by about 0.3 eV. Hybrid functionals perform better, in this case especially so B3LYP-D3. We do not have a direct experimental reference to compare to (rather, on the contrary, the value obtained in the work can serve as a reference for the experiment). However, the high barrier obtained here can be qualitatively supported by the fact that the hydrogen vibrations in positions 1-4 are observed experimentally,[51] suggesting that the hydrogen atoms diffuse from 1-4 to 1-2 rather slowly.

Second, this work demonstrates a protocol for calculating reaction barriers on non-conducting surfaces. The periodic HF and local MP2 with (A)VTZ-quality basis sets are expected to be already reasonably close to the basis set limit. OSV-based LMP2 calculations are much more robust than the PAO ones as concerns the balance of the virtual space between different points on the potential surface. The basis set limit can be calculated either by extrapolation of the OSV-LMP2 energies (the corresponding Dunning basis set can be used only for the fragments surrounding the reaction) or via an LMP2-F12 calculation. Since the implementation of the OSV-based periodic local F12 method is yet underway, for the PAO-based version of F12, one should use very big domains (e.g., iext = 2); otherwise, unbalanced results may be obtained.

When metal atoms are present, the standard frozen-core approximation may not be sufficiently accurate. In our case, the correlation contributions from the upper core of Al are sizable and should be evaluated. Another important correction is the CCSD(T) correction on top of MP2. In order to evaluate this correction, an embedded fragment approach is practical and very efficient. If all the interesting steps of the reaction involve only adsorbed species, the long-range dispersion is expected to cancel to a large extent in the energy differences, reducing the essential active region to a local space around the reacting species.

SUPPLEMENTARY MATERIAL

See the supplementary material for the specification of the structures, basis sets, and other computational parameters, as well as a detailed compilation of the obtained results.

ACKNOWLEDGMENTS

AUTHOR DECLARATIONS

Conflict of Interest

The authors have no conflict of interest to declare.

DATA AVAILABILITY

The data that support the findings of this study are available within the article and its supplementary material.

REFERENCES

[1]G.-J. Kroes, "Computational approaches to dissociative chemisorption on metals: Towards chemical accuracy," Phys. Chem. Chem. Phys. **23**, 8962 (2021).

[2]S. Heiden, D. Usvyat, and P. Saalfrank, "Theoretical surface science beyond gradient-corrected density functional theory: Water at α-Al$_2$O$_3$(0001) as a case study," J. Phys. Chem. C **123**, 6675 (2019).

[3]J. Řezáč, K. E. Riley, and P. Hobza, "S66: A well-balanced database of benchmark interaction energies relevant to biomolecular structures," J. Chem. Theory Comput. **7**, 2427–2438 (2011).

[4]M. Schütz, "Low-order scaling local electron correlation methods. III. Linear scaling local perturbative triples correction (T)," J. Chem. Phys. **113**, 9986–10001 (2000).

[5]M. Schütz and H.-J. Werner, "Low-order scaling local electron correlation methods. IV. Linear scaling local coupled-cluster (LCCSD)," J. Chem. Phys. **114**, 661–681 (2001).

[6]H.-J. Werner and M. Schütz, "An efficient local coupled cluster method for accurate thermochemistry of large systems," J. Chem. Phys. **135**, 144116 (2011).

[7]C. Riplinger and F. Neese, "An efficient and near linear scaling pair natural orbital based local coupled cluster method," J. Chem. Phys. **138**, 034106 (2013).

[8]C. Riplinger, B. Sandhoefer, A. Hansen, and F. Neese, "Natural triple excitations in local coupled cluster calculations with pair natural orbitals," J. Chem. Phys. **139**, 134101 (2013).

[9]M. Schütz, O. Masur, and D. Usvyat, "Efficient and accurate treatment of weak pairs in local CCSD(T) calculations. II. Beyond the ring approximation," J. Chem. Phys. **140**, 244107 (2014).

[10]M. Schwilk, D. Usvyat, and H.-J. Werner, "Communication: Improved pair approximations in local coupled-cluster methods," J. Chem. Phys. **142**, 121102 (2015).

[11]Q. Ma and H.-J. Werner, "Scalable electron correlation methods. 5. Parallel perturbative triples correction for explicitly correlated local coupled cluster with pair natural orbitals," J. Chem. Theory Comput. **14**, 198 (2018).

[12]P. R. Nagy, G. Samu, and M. Kállay, "Optimization of the linear-scaling local natural orbital CCSD(T) method: Improved algorithm and benchmark applications," J. Chem. Theory Comput. **14**, 4193 (2018).

[13]Th. Gruber, K. Liao, Th. Tsatsoulis, F. Hummel, and A. Grüneis, "Applying the coupled-cluster ansatz to solids and surfaces in the thermodynamic limit," Phys. Rev. X **8**, 021043 (2018).

[14]J. McClain, Q. Sun, G. K.-L. Chan, and T. C. Berkelbach, "Gaussian-based coupled-cluster theory for the ground-state and band structure of solids," J. Chem. Theory Comput. **13**, 1209 (2017).

[15]A. Hermann and P. Schwerdtfeger, "Equation of state for solid neon from quantum theory," Phys. Rev. B **80**, 064106 (2009).

[16]J. Yang, W. Hu, D. Usvyat, D. Matthews, M. Schütz, and G. K. Chan, "Ab initio determination of the crystalline benzene lattice energy to sub-kilojoule/mole accuracy," Science **345**, 640 (2014).

[17]H. Stoll, "Correlation energy of diamond," Phys. Rev. B **46**, 6700 (1992).

[18]B. Paulus, "The method of increments—A wavefunction-based ab initio correlation method for solids," Phys. Rep. **428**, 1 (2006).

[19]E. Voloshina, D. Usvyat, M. Schütz, Y. Dedkov, and B. Paulus, "On the physisorption of water on graphene: A CCSD(T) study," Phys. Chem. Chem. Phys. **13**, 12041 (2011).

[20]S. J. Nolan, M. J. Gillan, D. Alfè, N. L. Allan, and F. R. Manby, "Calculation of properties of crystalline lithium hydride using correlated wave function theory," Phys. Rev. B **80**, 165109 (2009).

[21]C. Tuma and J. Sauer, "Treating dispersion effects in extended systems by hybrid MP2:DFT calculations—Protonation of isobutene in zeolite ferrierite," Phys. Chem. Chem. Phys. **8**, 3955 (2006).

[22]C. Müller and D. Usvyat, "Incrementally corrected periodic local MP2 calculations: I. The cohesive energy of molecular crystals," J. Chem. Theory Comput. **9**, 5590 (2013).

[23]D. Usvyat, "High precision quantum-chemical treatment of adsorption: Benchmarking physisorption of molecular hydrogen on graphane," J. Chem. Phys. **143**, 104704 (2015).

[24]A. D. Boese and P. Saalfrank, "CO molecules on a NaCl(100) surface: Structures, energetics, and vibrational Davydov splittings at various coverages," J. Phys. Chem. C **120**, 12637 (2016).

[25]T. Tsatsoulis, F. Hummel, D. Usvyat, M. Schütz, G. H. Booth, S. S. Binnie, M. J. Gillan, D. Alfè, A. Michaelides, and A. Grüneis, "A comparison between quantum chemistry and quantum Monte Carlo techniques for the adsorption of water on the (001) LiH surface," J. Chem. Phys. **146**, 204108 (2017).

[26]M. Schütz, L. Maschio, A. J. Karttunen, and D. Usvyat, "Exfoliation energy of black phosphorus revisited: A coupled cluster benchmark," J. Phys. Chem. Lett. **8**, 1290 (2017).

[27] M. Alessio, F. A. Bischoff, and J. Sauer, "Chemically accurate adsorption energies for methane and ethane monolayers on the MgO(001) surface," Phys. Chem. Chem. Phys. **20**, 9760 (2018).

[28] M. Alessio, D. Usvyat, and J. Sauer, "Chemically accurate adsorption energies: CO and H_2O on the MgO(001) surface," J. Chem. Theory Comput. **15**, 1329 (2019).

[29] N. Govind, Y. A. Wang, A. J. R. da Silva, and E. A. Carter, "Accurate ab initio energetics of extended systems via explicit correlation embedded in a density functional environment," Chem. Phys. Lett. **295**, 129 (1998).

[30] T. Klüner, N. Govind, Y. A. Wang, and E. A. Carter, "Periodic density functional embedding theory for complete active space self-consistent field and configuration interaction calculations: Ground and excited states," J. Chem. Phys. **116**, 42 (2002).

[31] J. Neugebauer, M. J. Louwerse, E. J. Baerends, and T. A. Wesolowski, "The merits of the frozen-density embedding scheme to model solvatochromic shifts," J. Chem. Phys. **122**, 094115 (2005).

[32] P. Huang and E. A. Carter, "Self-consistent embedding theory for locally correlated configuration interaction wave functions in condensed matter," J. Chem. Phys. **125**, 084102 (2006).

[33] A. S. P. Gomes, Ch. R. Jacob, and L. Visscher, "Calculation of local excitations in large systems by embedding wave-function theory in density-functional theory," Phys. Chem. Chem. Phys. **10**, 5353 (2008).

[34] F. R. Manby, M. Stella, J. D. Goodpaster, and Th. F. Miller, "A simple, exact density-functional-theory embedding scheme," J. Chem. Theory Comput. **8**, 2564 (2012).

[35] T. A. Barnes, J. D. Goodpaster, F. R. Manby, and Th. F. Miller, "Accurate basis set truncation for wavefunction embedding," J. Chem. Phys. **139**, 024103 (2013).

[36] F. Libisch, C. Huang, and E. A. Carter, "Embedding for bulk systems using localized atomic orbitals," Acc. Chem. Res. **47**, 2768 (2014).

[37] J. D. Goodpaster, T. A. Barnes, F. R. Manby, and Th. F. Miller, "Accurate and systematically improvable density functional theory embedding for correlated wavefunctions," J. Chem. Phys. **140**, 18A507 (2014).

[38] P. K. Tamukong, Y. G. Khait, and M. R. Hoffmann, "Density differences in embedding theory with external orbital orthogonality," J. Phys. Chem. A **118**, 9182 (2014).

[39] B. Hégely, P. R. Nagy, G. G. Ferenczy, and M. Kállay, "Exact density functional and wave function embedding schemes based on orbital localization," J. Chem. Phys. **145**, 064107 (2016).

[40] F. Libisch, M. Marsman, J. Burgdörfer, and G. Kresse, "Embedding for bulk systems using localized atomic orbitals," J. Chem. Phys. **147**, 034110 (2017).

[41] T. Culpitt, K. R. Brorsen, and S. Hammes-Schiffer, "Communication: Density functional theory embedding with the orthogonality constrained basis set expansion procedure," J. Chem. Phys. **146**, 211101 (2017).

[42] D. V. Chulhai and J. D. Goodpaster, "Projection-based correlated wave function in density functional theory embedding for periodic systems," J. Chem. Theory Comput. **14**, 1928 (2018).

[43] P. J. Bygrave, N. L. Allan, and F. R. Manby, "The embedded many-body expansion for energetics of molecular crystals," J. Chem. Phys. **137**, 164102 (2012).

[44] O. Masur, M. Schütz, L. Maschio, and D. Usvyat, "Fragment-based direct-local-ring-coupled-cluster doubles treatment embedded in the periodic Hartree–Fock solution," J. Chem. Theory Comput. **12**, 5145 (2016).

[45] D. Usvyat, L. Maschio, and M. Schütz, "Periodic and fragment models based on the local correlation approach," Wiley Interdiscip. Rev.: Comput. Mol. Sci. **8**, e1357 (2018).

[46] H.-H. Lin, L. Maschio, D. Kats, D. Usvyat, and T. Heine, "Fragment-based restricted active space configuration interaction with second-order corrections embedded in periodic Hartree–Fock wave function," J. Chem. Theory Comput. **16**, 7100 (2020).

[47] T. Schäfer, F. Libisch, G. Kresse, and A. Grüneis, "Local embedding of coupled cluster theory into the random phase approximation using plane waves," J. Chem. Phys. **154**, 011101 (2021).

[48] B. T. G. Lau, G. Knizia, and T. C. Berkelbach, "Regional embedding enables high-level quantum chemistry for surface science," J. Phys. Chem. Lett. **12**, 1104 (2021).

[49] J. Chen, N. A. Bogdanov, D. Usvyat, W. Fang, A. Michaelides, and A. Alavi, "The color center singlet state of oxygen vacancies in TiO_2," J. Chem. Phys. **153**, 204704 (2020).

[50] E. Christlmaier, D. Kats, A. Alavi, and D. Usvyat, "Full configuration interaction quantum Monte Carlo treatment of fragments embedded in a periodic mean field," J. Chem. Phys. (submitted) (2022).

[51] H. Kirsch, J. Wirth, Y. Tong, M. Wolf, P. Saalfrank, and R. K. Campen, "Experimental characterization of unimolecular water dissociative adsorption on α-alumina," J. Phys. Chem. C **118**, 13623 (2014).

[52] R. Dovesi, A. Erba, R. Orlando, C. M. Zicovich-Wilson, B. Civalleri, L. Maschio, M. Rerat, S. Casassa, J. Baima, S. Salustro, and B. Kirtman, "Quantum-mechanical condensed matter simulations with crystal," Wiley Interdiscip. Rev.: Comput. Mol. Sci. **8**, e1360 (2018).

[53] T. H. Dunning, Jr., "Gaussian basis sets for use in correlated molecular calculations. I. The atoms boron through neon and hydrogen," J. Chem. Phys. **90**, 1007 (1989).

[54] L. Maschio, D. Usvyat, M. Schütz, and B. Civalleri, "Periodic local Møller–Plesset second order perturbation theory method applied to molecular crystals: Study of solid NH_3 and CO_2 using extended basis sets," J. Chem. Phys. **132**, 134706 (2010).

[55] K. Wolinski and P. Pulay, "Second-order Møller–Plesset calculations with dual basis sets," J. Chem. Phys. **118**, 9497 (2003).

[56] R. A. Kendall, T. H. Dunning, Jr., and R. J. Harrison, "Electron affinities of the first-row atoms revisited. Systematic basis sets and wave functions," J. Chem. Phys. **96**, 6796 (1992).

[57] D. Usvyat, L. Maschio, C. Pisani, and M. Schütz, "Second order local Møller-Plesset perturbation theory for periodic systems: The CRYSCOR code," Z. Phys. Chem. **224**, 441 (2010).

[58] K. A. Peterson and T. H. Dunning, "Accurate correlation consistent basis sets for molecular core–valence correlation effects: The second row atoms Al–Ar, and the first row atoms B–Ne revisited," J. Chem. Phys. **117**, 10548 (2002).

[59] M. Schütz, G. Hetzer, and H.-J. Werner, "Low-order scaling local electron correlation methods. I. Linear scaling local MP2," J. Chem. Phys. **111**, 5691 (1999).

[60] C. Pisani, L. Maschio, S. Casassa, M. Halo, M. Schütz, and D. Usvyat, "Periodic local MP2 method for the study of electronic correlation in crystals: Theory and preliminary applications," J. Comput. Chem. **29**, 2113 (2008).

[61] O. Masur, D. Usvyat, and M. Schütz, "Efficient and accurate treatment of weak pairs in local CCSD(T) calculations," J. Chem. Phys. **139**, 164116 (2013).

[62] S. Saebø and P. Pulay, "Local configuration interaction: An efficient approach for larger molecules," Chem. Phys. Lett. **113**, 13 (1985).

[63] J. Yang, Y. Kurashige, F. R. Manby, and G. K. L. Chan, "Tensor factorizations of local second-order Møller–Plesset theory," J. Chem. Phys. **134**, 044123 (2011).

[64] D. Usvyat, L. Maschio, and M. Schütz, "Periodic local MP2 method employing orbital specific virtuals," J. Chem. Phys. **143**, 102805 (2015).

[65] M. Schütz, D. Usvyat, M. Lorenz, C. Pisani, L. Maschio, S. Casassa, and M. Halo, "Density fitting for correlated calculations in periodic systems," in *Accurate Condensed-Phase Quantum Chemistry*, edited by F. R. Manby (CRC Press, Boca Raton, FL, 2010), p. 29.

[66] D. Usvyat, "Linear-scaling explicitly correlated treatment of solids: Periodic local MP2-F12 method," J. Chem. Phys. **139**, 194101 (2013).

[67] F. R. Manby and P. J. Knowles, "The Poisson equation in the Kohn-Sham Coulomb problem," Phys. Rev. Lett. **87**, 163001 (2001).

[68] F. R. Manby, P. J. Knowles, and A. W. Lloyd, "The Poisson equation in density fitting for the Kohn-Sham Coulomb problem," J. Chem. Phys. **115**, 9144 (2001).

[69] F. Weigend, A. Köhn, and C. Hättig, "Efficient use of the correlation consistent basis sets in resolution of the identity MP2 calculations," J. Chem. Phys. **116**, 3175 (2002).

[70] T. Helgaker, W. Klopper, H. Koch, and J. Noga, "Basis-set convergence of correlated calculations on water," J. Chem. Phys. **106**, 9639 (1997).

[71] H.-J. Werner, P. J. Knowles, F. R. Manby, J. A. Black, K. Doll, A. Heßelmann, D. Kats, A. Köhn, T. Korona, D. A. Kreplin, Q. Ma, Th. F. Miller, A. Mitrushchenkov,

K. A. Peterson, I. Polyak, G. Rauhut, and M. Sibaev, "The Molpro quantum chemistry package," J. Chem. Phys. **152**, 144107 (2020).

[72] P. J. Knowles and N. C. Handy, "A determinant based full configuration interaction program," Comput. Phys. Commun. **54**, 75 (1989).

[73] D. Kats and F. R. Manby, "Communication: The distinguishable cluster approximation," J. Chem. Phys. **139**, 021102 (2013).

[74] D. Kats, D. Kreplin, H.-J. Werner, and F. R. Manby, "Accurate thermochemistry from explicitly correlated distinguishable cluster approximation," J. Chem. Phys. **142**, 064111 (2015).

[75] D. Kats, "Improving the distinguishable cluster results: Spin-component scaling," Mol. Phys. **116**, 1435 (2018).

[76] C. Hampel and H. J. Werner, "Local treatment of electron correlation in coupled cluster theory," J. Chem. Phys. **104**, 6286 (1996).

[77] S. Tosoni and J. Sauer, "Accurate quantum chemical energies for the interaction of hydrocarbons with oxide surfaces: $CH_4/MgO(001)$," Phys. Chem. Chem. Phys. **12**, 14330 (2010).

[78] A. D. Boese and J. Sauer, "Accurate adsorption energies of small molecules on oxide surfaces: $CO–MgO(001)$," Phys. Chem. Chem. Phys. **15**, 16481 (2013).

[79] D. Usvyat, K. Sadeghian, L. Maschio, and M. Schütz, "Geometrical frustration of an argon monolayer adsorbed on the MgO(100) surface: An accurate periodic *ab initio* study," Phys. Rev. B **86**, 045412 (2012).